International Journal for Modern Trends in Science and Technology
Volume 12, Issue 05, pages 452-465
ISSN: 2455-3778 online
Available online at: http://www.ijmtst.com/vol12issue05.html
DOI: https://doi.org/10.5281/zenodo.20560950

Bidirectional EV Onboard Charging Using a Power-Quality-Optimized Interleaved Totem-Pole and Push–Pull Converter for V2G Applications

Dr. J. Srinu Naick | D. Anil Kumar | Y. Siva Kumar Reddy | B. Chandu | Y. Hinduja

Department of Electrical and Electronics Engineering, Chadalawada Ramanamma Engineering College, Tirupati, Andhra Pradesh, India.

To Cite this Article
Dr. J. Srinu Naick, D. Anil Kumar, Y. Siva Kumar Reddy, B. Chandu & Y. Hinduja (2026). Bidirectional EV Onboard Charging Using a Power-Quality-Optimized Interleaved Totem-Pole and Push–Pull Converter for V2G Applications, International Journal for Modern Trends in Science and Technology, 12(05), 452-465. https://doi.org/10.5281/zenodo.20568074

Article Info
Received: 07 May 2026; Revised: 26 May 2026; Accepted: 30 May 2026.

KEYWORDS

Bidirectional Onboard Charger, Interleaved Totem-Pole Converter, Push–Pull Converter, Power Quality Improvement, Vehicle-to-Grid (V2G), Electric Vehicle Charging, Power Factor Correction.

ABSTRACT

This study offers a power-quality-enhanced bidirectional interleaved totem-pole converter–based onboard charger (OBC) for electric vehicle (EV) applications to reduce power conversion stages, improve efficiency, and enable V2G operation. A diode bridge rectifier (DBR), front-end boost converter for power factor correction (PFC), and back-end isolated push–pull converter for battery charging are used in two-stage OBC systems. These structures are effective but have greater conduction losses, component count, power density, and unidirectional power flow, restricting operation to grid-to-vehicle (G2V) mode. A bidirectional interleaved totem-pole AC–DC converter with fully active switches substitutes the DBR, boost PFC, and push–pull stages to overcome these restrictions. In typical push–pull converters, transformer secondary passive diode rectifiers limit power flow to one direction. In contrast, the suggested architecture uses actively controlled switches on both converter sides to govern bidirectional energy flow between the grid and the EV battery. This arrangement minimizes component count, eliminates diode conduction losses, and delivers near-unity power factor and minimal input current harmonic distortion. The interleaved construction reduces current ripple, improves heat distribution, and boosts power density. The dc-bus voltage, constant-current/constant-voltage (CC/CV) battery charging, and power quality under different grid and load circumstances are regulated by an innovative control approach. Simulations show that the suggested OBC improves power factor, switching and conduction losses, efficiency, and stable bidirectional G2V/V2G operation compared to unidirectional OBC topologies, making it a suitable option for next-generation EV charging and grid-interactive applications.

1. Introduction

Innovative power electronic converters have been greatly impacted by the growing use of electric cars in contemporary transportation networks, allowing for more efficient management and conversion of energy. To charge the electric car's battery, onboard chargers are essential, as they allow power to be transferred from the grid to the vehicle. Boost type power factor correction converters and isolated dc dc converters are the usual components of conventional onboard charger topologies, which for battery charging normally use a two-stage setup. Following this is a diode bridge rectifier. Increased conduction losses, large passive components, a greater component count, and decreased overall efficiency are some of the inherent disadvantages of this technique, despite its widespread use owing to its simplicity and dependability [1]. Additionally, the implementation of vehicle-to-grid capability is hindered by the existence of passive diode rectifiers, which limit the power flow to unidirectional operation and keep the system limited to grid-to-vehicle mode only [2]. The integration of smart grids and the development of sustainable energy systems have led many to see electric cars as a kind of distributed energy storage that can communicate with the grid. Electric cars may assist with grid operations including voltage stability, frequency regulation, and peak load shaving thanks to vehicle to grid technology, which allows electricity to flow in both directions from the battery to the grid [3]. Because of this paradigm change, it is critical to provide onboard chargers that can charge and discharge rapidly without sacrificing system dependability or power quality. Since they are ill-equipped to manage reverse power flow and have limited functionality, traditional unidirectional charger topologies are unsuitable for such uses [4]. A lot of work has gone into studying how to make onboard chargers' ac dc conversion stages work better and more efficiently in recent years. To avoid using a diode bridge rectifier and instead use actively controlled switches for rectification, the totem pole converter has become a potential architecture. This leads to better efficiency and lower conduction losses, especially at high power levels [5]. Totem pole converters are made even better by using wide bandgap semiconductor devices like gallium nitride or silicon carbide, which allow for high frequency switching, lower switching losses, and better thermal properties [6]. Despite these benefits, the performance and reliability of single phase totem pole converters may be affected by problems such as current ripple, electromagnetic interference, and uneven heat distribution [7]. Power converter design has extensively used interleaving methods to circumvent these obstacles. With interleaved converters, the input and output current ripple is minimized, efficiency is increased, and thermal management is enhanced because of the many parallel phases that work with phase shifted switching signals [8]. For onboard charger applications where size and weight are paramount, the interleaving technique is extremely appropriate since it enables reduced passive components and greater power density [9]. It is feasible to create a small, efficient, and power-quality-enhancing ac-dc conversion stage by integrating the benefits of totem pole topology with interleaving [10]. The onboard charger's galvanic isolation and regulation of the charging process for the batteries are both handled by the isolated dc dc converter stage. Because of its straightforward design, transformer efficiency, and applicability to medium power applications, the push-pull converter is one of the most used isolated converter topologies [11]. Traditional designs, however, restrict the converter to operating in just one direction due to the secondary side's usage of diode rectifiers. Because of this, the system can't handle bidirectional energy transmission, which is crucial for applications that connect vehicles to the grid [12]. A modification to the push-pull converter that allows for bidirectional operation—that is, controlled energy transfer between the grid and the car battery—is possible by substituting actively controlled switches for passive rectifiers [13]. Because of the detrimental effects on the grid and violations of regulatory requirements like IEEE 519, power quality is an essential component of onboard charger design. To achieve a power factor close to unity and minimal total harmonic distortion, the input current must be sinusoidal and in phase with the grid voltage [14]. To accomplish these goals while maintaining stable operation under changing grid and load circumstances, advanced control techniques are necessary. There has been a lot of research on methods that can improve the dynamic response and resilience of power converters, such as adaptive control, predictive control, and proportional integral control [15]. Efficient battery charging under constant current and constant voltage modes is also dependent on the ac dc and dc dc stages

coordinating with one another [16]. Smart grid infrastructure that incorporates bidirectional onboard chargers increases electric cars' potential by letting them take part in grid support services. During times of low demand, electric cars may store energy and release it back into the grid during times of high demand [17]. Both grid stability and the usage of renewable energy sources like wind and solar are enhanced by this. Multiple studies have shown that vehicle-to-grid technology has the capacity to aid in the integration of renewable energy sources, decrease energy prices, and improve system dependability [18]. High power quality and efficient bidirectional power flow are prerequisites for dependable V2G operation, which in turn necessitates sophisticated converter topologies [19]. For on-board charging applications in electric vehicles, this article suggests a bidirectional interleaved totem pole and push pull converter that optimizes power quality. By doing away with the diode bridge rectifier and other unnecessary conversion stages, the suggested architecture improves efficiency and cuts losses. Actively regulated switches in both the ac dc and dc dc phases allow for continuous bidirectional power flow, while interleaving reduces current ripple and improves thermal performance [20]. To keep the power factor close to unity, manage the dc bus voltage, and charge the batteries correctly in both constant current and constant voltage modes, a sophisticated control technique is used. Enhanced efficiency, less harmonic distortion, and dependable operation in both grid-to-vehicle and vehicle-to-grid modes are all shown in the simulation results, validating the success of the proposed system.

2. System Configuration

An isolated push-pull DC-DC converter for electric vehicle (EV) battery interface, a solar PV-based DC-DC boost converter, and an AC-DC totem-pole converter make up the suggested system. The OBC may charge both ways. Improved efficiency and power quality are two goals of the setup's design process as it pertains to grid-to-vehicle (G2V) and vehicle-to-grid (V2G) operations. An AC-DC totem-pole voltage source converter (VSC) with input inductor Lf and switches S1–S4 is used on the grid side. Maintaining sinusoidal and phase-locked grid current (Is) is how this converter corrects power factor. Additionally, it controls the DC-link voltage (Vdc) across capacitor Cdc, which reduces conduction losses and does away with the need for a diode bridge. A DC-DC boost converter—consisting of an inductor, switch, diode, and capacitor—connects a solar PV system. In order to integrate renewable energy sources and fulfill the load demand, this step increases the PV voltage (Vpv) and sends electricity to the DC-link. An isolated push-pull converter, housing high-frequency transformers and switches G1-G4, receives power from the DC-link. Bidirectional energy transmission between the DC-link and the EV battery is made possible by using active switches on both the main and secondary sides, which is an innovation compared to typical systems. This enables the ability to charge and discharge. An LC filter (consisting of Ls and Cs) ensures steady operation by smoothing the voltage and current provided to the EV battery at the output. You may manage the charging and draining of the battery by adjusting the voltage (Vev) and current (Iev). Enabling effective energy management, decreased losses, and dependable bidirectional operation appropriate for current EV and smart grid applications, the system connects grid, PV, and EV over a unified DC-link.

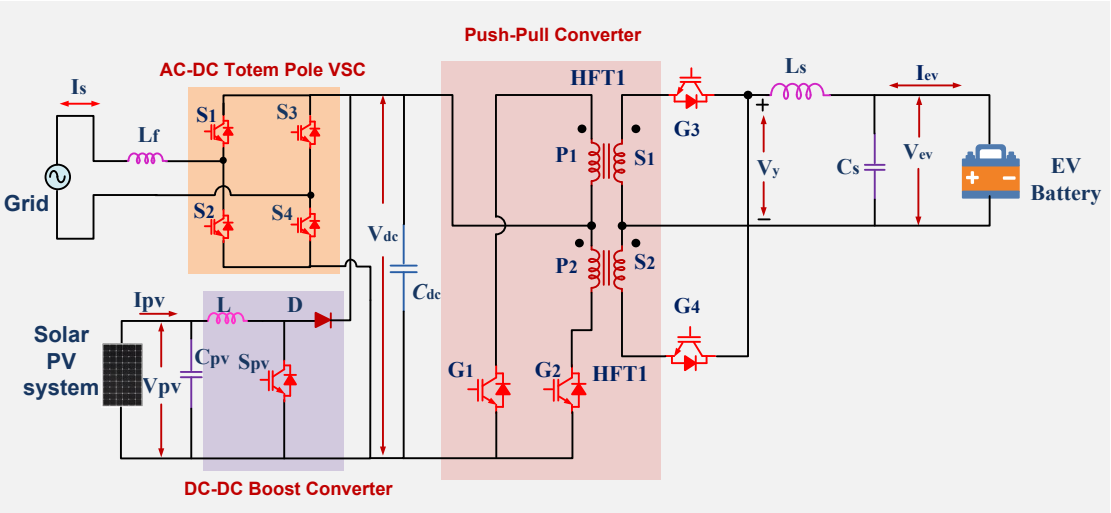

Fig. 1. Proposed Bidirectional OBC with Solar PV and EV Battery Integration

3. Modeling and Design of proposed system Configuration

A. Single-Diode Solar PV System

Because it accurately represents PV properties under different environmental circumstances, the single-diode equivalent circuit is often used to mimic the solar photovoltaic system. Here, the photovoltaic cell is represented by a current source, a diode, and series and shunt resistances, which are used to account for internal losses. The current that the PV system produces at its output is

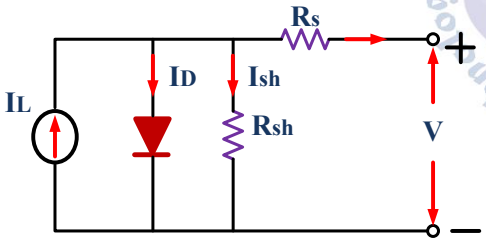

Fig. 2 equivalent model of PV solar.

$$I_{pv} = I_{Ph} - I_0\left[\exp\left(\frac{V_{pv}+I_{pv}R_s}{\alpha V_t}\right) - 1\right] - \frac{V_{pv}+I_{pv}R_s}{R_{sh}} \quad (1)$$

The generated photocurrent depends on solar irradiance and temperature, and is given by

$$I_{Ph} = \left[I_{sc.ref} + K_i\left(T - T_{ref}\right)\right]\frac{G}{G_{ref}} \quad (2)$$

The output power of the PV system is

$$P_{pv} = V_{pv}I_{pv} \quad (3)$$

The power-voltage characteristic of the PV panel exhibits a unique maximum power point (MPP) at which the power is maximum. This condition is defined by

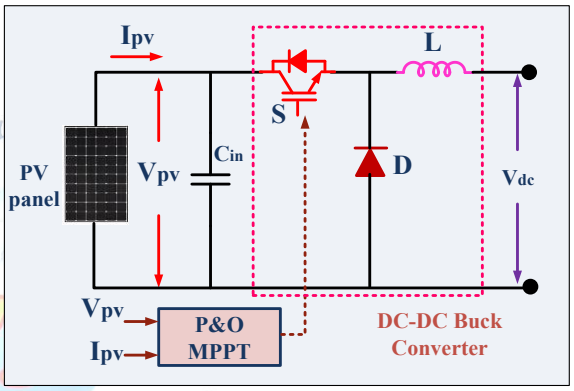

Fig. 3 solar PV P&O MPPT DC-DC Buck converter

$$\frac{dP}{dV} = 0 \quad (4)$$

Using a boost converter in conjunction with a maximum power point tracking (MPPT) algorithm guarantees that the PV system functions continuously at this maximum power point. In order to change the operating point, the boost converter regulates the duty cycle and increases the PV voltage. Here is the boost converter's voltage gain:

$$V_0 = \frac{V_{pv}}{1-D} \quad (5)$$

where D is the duty ratio. By varying D, the input voltage and current of the PV system are controlled.

The inductor and capacitor of the boost converter are designed based on ripple considerations. The inductance is given by

$$L = \frac{V_{pv}D}{\Delta I_L f_s}$$

$$L = \frac{V_{pv}D}{\Delta I_L f_s} \quad (6)$$

and the output capacitor is selected as

$$C = \frac{I_0 D}{\Delta V_o f_s} \quad (7)$$

B. P&O MPPT Boost Converter

The Perturb and Observe (P&O) MPPT algorithm is used to track the maximum power point. In this method, the PV voltage or duty cycle is slightly perturbed and the resulting change in power is observed. The power is calculated as

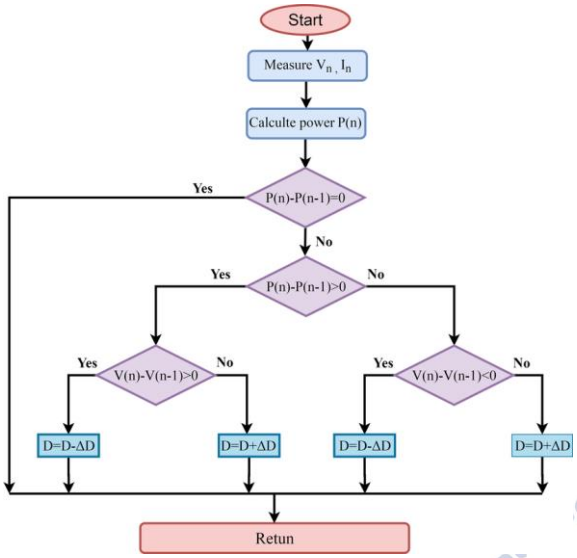

Fig.4 flow chart of P&O MPPT algorithm

$$P(k) = V(k)I(k) \quad (7)$$

The changes in power and voltage are given by

$$\Delta P = P(k) - P(K-1) \quad (8)$$

$$\Delta V = V(k) - V(k-1) \quad (9)$$

Based on these values, the duty cycle is updated as

$$D(k) = D(k-1) \pm \Delta D \quad (10)$$

The operating point shifts toward the maximum power point and the perturbation persists in the same direction if the power rises after perturbation. The direction is switched backwards when the electricity goes out. In sum, the P&O MPPT algorithm, boost converter, and single-diode PV model work together to maximize power output from the PV system regardless of temperature or irradiance. While the MPPT algorithm is constantly adjusting the operating point to ensure optimum performance, the boost converter regulates the voltage.

4. Isolated converter DC-DC Converters

A Bidirectional Isolated DC–DC Push–Pull Converter

Electric vehicle (EV) onboard chargers and energy storage systems often use a bidirectional isolated DC-DC push-pull converter architecture for regulated and efficient power transmission between two DC sources. Supporting both grid-to-vehicle (G2V) and vehicle-to-grid (V2G) operations, bidirectional converters allow energy transmission in both ways, in contrast to traditional converters that only allow unidirectional power flow. Using a center-tapped transformer, the push-pull converter achieves galvanic isolation, voltage matching, and enhanced safety in an isolated topology.

The use of diode rectifiers on the secondary side of traditional push-pull converters limits the direction of power flow. On the other hand, a bidirectional arrangement allows for reversible energy transmission by substituting these diodes with actively controlled switches. To improve efficiency and cut down on conduction losses, active switches are used. Factors like as load circumstances, switching frequency, duty cycle, and transformer turns ratio determine the converter's performance.

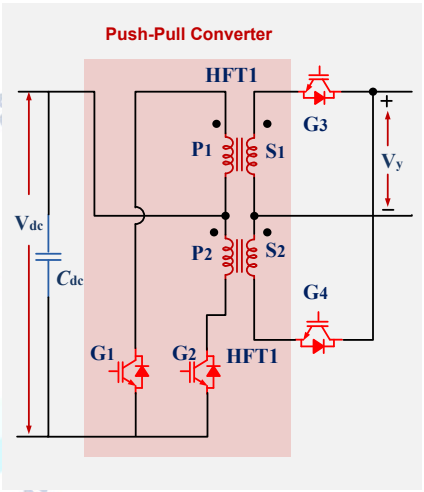

Fig. 5 Basic Push-Pull Converters

B. Working Principle with Fundamental Equations

The operation of the push–pull converter is based on alternate switching of two power switches connected to a center-tapped primary winding of a transformer. Each switch conducts for a duration defined by the duty cycle D, producing an alternating voltage across the transformer.

The instantaneous primary voltage is:

$$V_p(t) = V_{in} \quad (11)$$

The secondary voltage induced in the transformer is:

$$V_s(t) = \frac{N_s}{N_p} \cdot V_{in} \quad (12)$$

After rectification and filtering, the average output voltage becomes:

$$V_0 = 2 \cdot D \cdot \frac{N_s}{N_P} \cdot V_{in} \quad (13)$$

This factor of 2 appears because both halves of the transformer contribute during one switching cycle.

The output current is given by:

$$I_o = \frac{P_0}{V_0} \quad (14)$$

and input power is:

$$P_{in} = V_{in} \cdot I_{in} \quad (15)$$

Considering efficiency η:

$$\eta = \frac{P_0}{P_{in}} \quad (16)$$

Inductor and Ripple Equations

The output inductor smooths the current and its value is determined by allowable ripple:

$$L = \frac{V_L \cdot D}{\Delta I_L \cdot f_s} \quad (17)$$

where:

VL=Vs−Vo

ΔIL= inductor ripple current

fs = switching frequency

The ripple current is:

$$\Delta I_L = \frac{(V_s - V_0) \cdot D}{L \cdot f_s} \quad (18)$$

Output voltage ripple is:

$$\Delta V_o = \frac{I_0 \cdot D}{C \cdot f_s} \quad (19)$$

C. Operation of the Converter

The converter generates a high-frequency alternating current (AC) voltage across the transformer by reversing the primary-side switches S1 and S2. To keep current flowing through the main winding in a bidirectional fashion, only one switch is engaged at each switching period. Transformer core saturation may be avoided and efficient energy transfer can occur with this alternating excitation.

Substituting active switches for diodes on the secondary side allows for inversion in reverse operation and synchronous rectification in forward operation. By keeping the inductor current from ever dropping to zero, the converter may run in continuous conduction mode (CCM), which results in less loss and more consistent current flow.

The magnetizing current of the transformer is:

$$I_m = \frac{V_{in} \cdot D}{L_{in} \cdot f_s} \quad (20)$$

Where Lm is the magnetizing inductance.

D. Modes of Operation

a. Forward Mode (G2V Operation)

In forward mode, energy flows from the input DC source (grid/DC link) to the battery.

During Interval 1, switch S1 is ON:

- Primary voltage = Vin
- Secondary voltage = Ns/ Np*Vin
- Energy is transferred to the output

During **Interval 2**, switch S2 is ON:

- Current flows through the other half of the transformer
- Continuous energy transfer is maintained

The average output voltage is:

$$V_0 = 2D \cdot \frac{N_s}{N_p} \cdot V_{in} \quad (21)$$

The duty cycle is limited to:

$$D \leq 0.5 \quad (22)$$

to avoid transformer saturation.

b. Reverse Mode (V2G Operation)

In reverse mode, power flows from the battery to the grid/DC link.

Now the secondary side switches generate AC, and the transformer transfers energy to the primary side.

The voltage relationship becomes:

$$V_{in} = 2D \cdot \frac{N_p}{N_s} \cdot V_0 \quad (23)$$

The current direction reverses, and power delivered is:

$$P = V_0 \cdot I_0 = V_{in} \cdot I_{in} \quad (24)$$

In this mode, the converter behaves like an inverter followed by a rectifier.

c. Switch Stress and Transformer Considerations

The voltage stress on each switch is:

$$V_{switch} = 2 \cdot V_{in} \quad (25)$$

Peak current through switches:

$$I_{Peak} = I_0 \cdot \frac{N_P}{N_s} \quad (26)$$

Transformer design must satisfy:

$$B_{\max} = \frac{V_{in} \cdot D}{N_P \cdot A_e \cdot f_s} \quad (27)$$

where: Bmax = maximum flux density, A = core cross-sectional area

5. Modeling and Designing of Lithium-Ion Battery.

In modern power systems, Hybrid Energy Storage Systems (HESS) integrates multiple energy storage devices to enhance overall energy and power performance. Lithium-ion batteries, owing to their high energy density and efficiency, are widely utilized for sustained energy supply in such systems. The incorporation of multiple battery units facilitates improved operational flexibility and effective load management under varying conditions. This configuration enables enhanced load balancing, mitigates stress on individual battery units, and extends

overall battery lifespan. Furthermore, it improves system responsiveness and reliability, making it highly suitable for applications such as electric vehicle (EV) charging, renewable energy integration, and microgrid operations.

a. Lithium-Ion Battery Modeling

The lithium-ion battery used in the proposed system is modeled using a nonlinear dynamic equation that captures both charging and discharging characteristics. The battery terminal voltage is expressed as:

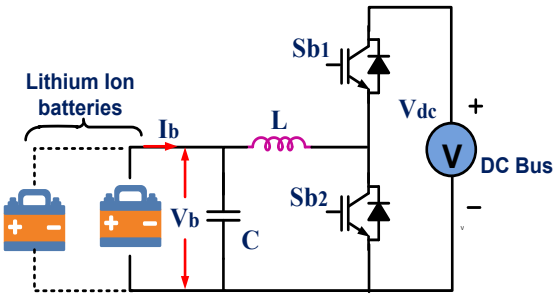

Fig.6 principle operation bidirectional dc-dc buck boost converter

$$E_B = E_0 - \frac{\mathrm{KQ}I_B}{Q - \int I_B \,\mathrm{dt}} - k\frac{Q}{Q - \int I_B\, dt} \int I_B \mathrm{dt} + \mathrm{A}\exp\left(-\mathrm{B}\int I_B\, dt\right) \quad (28)$$

where E_B represents the battery terminal voltage, E_0 is the constant open-circuit voltage, K denotes the polarization constant (V/Ah), Q is the maximum battery capacity (Ah), and IB is the battery current. The term $\int I_B\, dt$) represents the extracted capacity over time. The exponential term exp $(-\mathrm{B}\int I_B\, dt)$ models the voltage behavior in the exponential region of the battery discharge curve, where A and B are empirical constants. This model effectively captures the nonlinear voltage characteristics of lithium-ion batteries under varying load conditions. It accounts for polarization effects, capacity variation, and transient response during charging and discharging. The State of Charge (SoC) of the battery is estimated based on the integration of battery current, enabling accurate monitoring and control of energy storage units. The developed battery model is implemented for each BESS unit in the system, allowing decentralized control and SoC balancing across multiple batteries to enhance system reliability and lifespan.

6. Working and Operation of Totem-Pole PFC Converter and PV Boost Converter

The totem-pole power factor correction converter and the PV boost converter are connected across the common DC-link capacitor, while the EV-side converter and battery are considered as an equivalent load. The main objective of this stage is to regulate the DC-link voltage, shape the grid current into a sinusoidal waveform with low harmonic distortion, and simultaneously transfer the PV power to the DC link. During the positive half cycle of the grid voltage, switch S4 remains ON and switch S3 remains OFF. During the negative half cycle, switch S3 remains ON and switch S4 remains OFF. In both half cycles, switches S1, S2, and Spv are controlled according to the duty ratios of the PFC stage and PV boost stage.

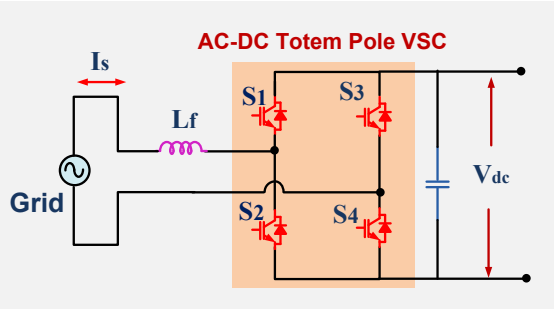

Fig. 7. Operation of Totem-Pole PFC Converter and PV Boost Converter

The grid-side inductor voltage is governed by

$$v_{L_f} = L_f \frac{di_s}{dt}$$

$$v_{L_f} = L_f \frac{di_s}{dt} \quad (29)$$

where Lf is the input inductor and is is the grid current. The PV-side boost inductor voltage is

$$v_{L_{pv}} = L_{pv} \frac{di_{pv}}{dt}$$

$$v_{L_{pv}} = L_{pv} \frac{di_{pv}}{d_t} \quad (30)$$

where Lpv is the PV boost inductor and ipv is the PV current. The DC-link capacitor dynamics can be written as

$$C_{dc} \frac{dV_{dc}}{dt} = i_{dc,in} - i_{dc,out}$$

$$C_{dc} \frac{dV_{dc}}{dt} = i_{dc.in} - i_{dC,out} \quad (31)$$

where Vdc is the DC-link voltage, idc,in is the current supplied by the grid and PV stages, and idc,out is the current drawn by the EV-side converter.

During the positive half cycle, the operation can be explained using the three switching states given in Table II.

In State 1, switches S2, S4, and Spv are ON, while S1 and S3 are OFF. In this condition, the grid-side inductor Lf is energized through the path formed by the source and active switches, and the PV inductor Lpv is also

energized because Spv is ON. Hence, the inductor voltages are

$$v_{L_f} = v_s$$

$$v_{L_f} = v_s \quad (32)$$

$$v_{L_{pv}} = V_{pv}$$

$$v_{L_{pv}} = V_{pv} \quad (33)$$

Thus, both inductors store energy and their currents increase linearly as

$$\frac{di_s}{dt} = \frac{v_s}{L_f}$$

$$\frac{di_s}{dt} = \frac{v_s}{L_f} \quad (34)$$

$$\frac{di_{pv}}{dt} = \frac{V_{pv}}{L_{pv}}$$

$$\frac{di_{pv}}{dt} = \frac{V_{pv}}{L_{pv}} \quad (35)$$

where vs is the instantaneous grid voltage and Vpv is the PV voltage.

In **State 2**, switches S1, S4, and Spv are ON, while S2 and S3 are OFF. In this state, the grid-side inductor releases energy to the DC-link capacitor and load, while the PV inductor continues charging because Spv is still ON. Therefore, the inductor voltages become

$$v_{L_f} = v_s - V_{dc}$$

$$v_{L_f} = v_s - V_{dc} \quad (36)$$

$$v_{L_{pv}} = V_{pv}$$

$$v_{L_{pv}} = V_{pv} \quad (37)$$

and the current slopes are

$$\frac{di_s}{dt} = \frac{v_s - V_{dc}}{L_f}$$

$$\frac{di_s}{dt} = \frac{v_s - V_{dc}}{L_f} \quad (38)$$

$$\frac{di_{pv}}{dt} = \frac{V_{pv}}{L_{pv}}$$

$$\frac{di_{pv}}{dt} = \frac{V_{pv}}{L_{pv}} \quad (39)$$

Since generally Vdc>vs, the grid inductor current decreases in this interval, transferring stored energy to the DC-link.

In **State 3**, switches S1 and S4 are ON, Spv is OFF, and S2 , S3 are OFF. In this condition, the grid-side inductor continues to transfer energy to the DC link, while the PV boost inductor releases its stored energy through the diode to the DC-link capacitor. Hence,

$$v_{L_f} = v_s - V_{dc}$$

$$v_{L_f} = v_s - V_{dc} \quad (40)$$

$$v_{L_{pv}} = V_{pv} - V_{dc}$$

$$v_{L_{pv}} = V_{pv} - V_{dc} \quad (41)$$

The corresponding current slopes are

$$\frac{di_s}{dt} = \frac{v_s - V_{dc}}{L_f}$$

$$\frac{di_s}{dt} = \frac{v_s - V_{dc}}{L_f} \quad (42)$$

$$\frac{di_{pv}}{dt} = \frac{V_{pv} - V_{dc}}{L_{pv}}$$

$$\frac{di_{pv}}{dt} = \frac{V_{pv} - V_{dc}}{L_{pv}} \quad (43)$$

Since the PV boost converter operates in boost mode, normally Vdc>Vpv, so the PV inductor current decreases while delivering power to the DC link.

Applying the volt-second balance principle to the grid-side inductor over one switching period gives

$$d_1(v_s) + (1 - d_1)(v_s - V_{dc}) = 0$$

$$d_1(v_s) + (1 - d_1)(v_5 - V_{dc}) = 0 \quad (44)$$

which simplifies to

$$V_{dc} = \frac{v_s}{1 - d_1}$$

$$V_{dc} = \frac{v_s}{1-d_1} \quad (45)$$

where d1 is the duty ratio associated with the PFC switching action. Similarly, for the PV boost inductor, volt-second balance gives

$$d_{pv}(V_{pv}) + (1 - d_{pv})(V_{pv} - V_{dc}) = 0$$

$$d_{pv}(V_{pv}) + (1 - d_{pv})(V_{pv} - V_{dc}) = 0 \quad (46)$$

which yields

$$V_{dc} = \frac{V_{pv}}{1 - d_{pv}}$$

$$V_{dc} = \frac{V_{pv}}{1-dpv} \quad (47)$$

where dpv is the duty ratio of the PV boost switch Spv.

The average grid current is controlled to follow the grid voltage reference for power factor correction. Therefore,

$$i_s^* = \frac{2P^*}{V_m} \sin \omega t$$

$$i_s^* = \frac{2p^*}{V_{in}} \sin \omega t \quad (48)$$

where is∗ is the reference grid current, P∗ is the reference input power, Vm is the peak grid voltage, and ω is the angular frequency. This ensures that the input current remains sinusoidal and in phase with the supply voltage, resulting in near-unity power factor.

The PV output power is given by

$$P_{pv} = V_{pv} I_{pv}$$

$$P_{pv} = V_{pv} I_{pv} \quad (49)$$

and this power is transferred to the DC link through the boost converter. The total power at the DC link can be expressed as

$$P_{dc} = P_{grid} + P_{pv}$$

$$P_{dc} = P_{grid} + P_{pv} \quad (50)$$

ignoring converter losses. This combined power supports the EV-side load and maintains the DC-link voltage constant. During the negative half cycle, the operation is similar, except that S3 remains ON and S4 remains OFF. The switching behavior of S1, S2, and Spv follows the same principle. Thus, the converter achieves symmetrical operation in both half cycles while maintaining PFC action and PV power injection. Overall, the totem-pole PFC converter shapes the grid current and regulates the DC-link voltage, whereas the PV boost converter extracts solar power and feeds it into the same DC link. The coordinated switching of S1, S2, S3, S4, and Spv enables simultaneous grid interfacing, PV power transfer, and efficient supply to the EV charging stage.

7. Controller designing of Totem Pole Converter

The control of the single-phase totem-pole converter is based on a two-loop control structure, consisting of an outer DC-link voltage control loop and an inner grid current control loop. The objective of the controller is to regulate the DC-link voltage while ensuring that the input current is sinusoidal and in phase with the grid voltage, achieving unity power factor.

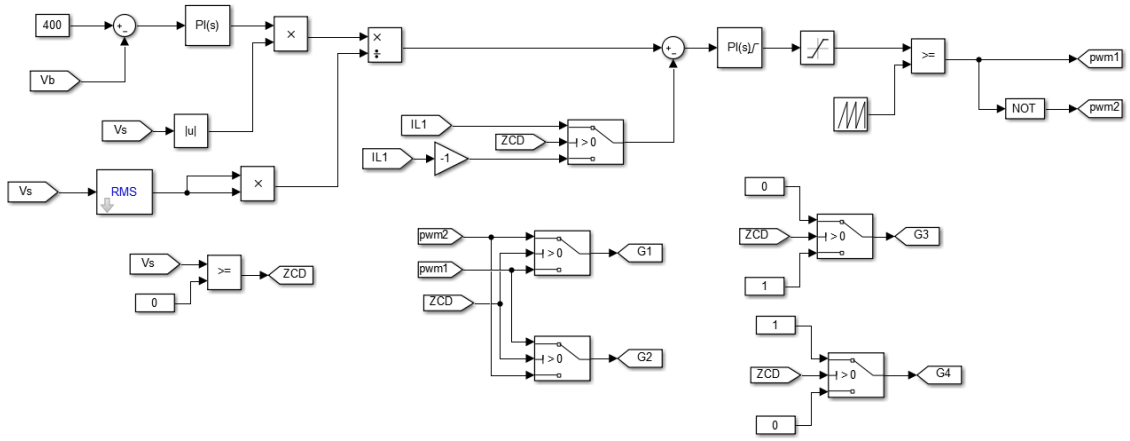

Fig. 8. Control Strategy of Single-Phase Totem-Pole PFC Converter

A. Outer Voltage Control Loop

The DC-link voltage is regulated by comparing the reference voltage Vdcref with the measured DC-link voltage Vdc. The error is given by

$$e_v = V_{dc}^{ref} - V_{dc}$$

$$e_v = V_{dc}^{ref} - V_{dc} \quad (51)$$

This error is processed through a PI controller to generate the reference current magnitude:

$$I_{ref} = K_p e_v + K_i \int e_v \, dt$$

$$I_{ref} = K_p e_v + k_i \int e_v dt \quad (52)$$

This output represents the amplitude of the reference grid current required to maintain the DC-link voltage.

B. Reference Current Generation

The instantaneous grid voltage vs is normalized using its RMS value to generate a unit sinusoidal signal:

$$u_s = \frac{v_s}{V_{s,rms}}$$

$$u_s = \frac{v_s}{V_{5,rms}} \quad (53)$$

The reference current is then obtained as

$$i_s^* = I_{ref} \cdot u_s$$

$$i_s^* = I_{ref} \cdot u_s \quad (54)$$

This ensures that the reference current follows the grid voltage waveform, achieving unity power factor operation.

C. Inner Current Control Loop

The actual grid current is is compared with the reference current is∗, and the error is given by

$$e_i = i_s^* - i_s$$

$$e_i = i_s^* - i_s \quad (55)$$

This signal represents the required voltage across the inductor to shape the current.

D. PWM Generation

The control signal is compared with a high-frequency carrier waveform to generate PWM pulses:

$$\text{PWM} = \begin{cases} 1, & v_{control} > v_{carrier} \\ 0, & \text{otherwise} \end{cases}$$

$$PWM = \begin{cases} 1, & v_{control} > v_{carrier} \\ 0, & otherwise \end{cases} \quad (56)$$

The generated PWM signals are used to control switches S1 and S2.

E. Switching Logic

The operation of switches S3 and S4 depends on the polarity of the grid voltage:

- For positive half cycle (vs>0):

$$S_4 = ON, \quad S_3 = OFF$$

$$S_4 = ON$$

$$S_3 = OFF \quad (57)$$

- For negative half cycle (vs<0):

$$S_3 = ON, \quad S_4 = OFF$$

$$S_3 = ON, \; S_4 = OFF \quad (58)$$

The complementary switching of S1 and S2 is given by:

$$S_2 = \overline{S_1}$$

$$s_2 = \bar{s}_1 \quad (59)$$

F. Inductor Current Dynamics

The grid-side inductor voltage is given by

$$v_L = L\frac{di_s}{dt}$$

$$v_L = L\frac{di_s}{dt} \quad (60)$$

During switching:

- When switch is ON:

$$v_L = L\frac{di_s}{dt}$$

$$V_L = L\frac{di_s}{dt} \quad (61)$$

During switching:

- When switch is ON:

$$v_L = v_s$$

$$v_L = v_s \quad (62)$$

- When switch is OFF:

$$v_L = v_s - V_{dc}$$

$$v_L = v_s - V_{dC} \quad (63)$$

8. Simulation Results and Discussion

A. Performance Analysis of the Proposed Bidirectional EV Onboard Charger

Based on the interleaved totem-pole front-end converter and bidirectional push-pull converter, the simulation results confirm the performance of the proposed bidirectional EV onboard charger under varied operating situations. A steady single-phase input supply is confirmed by the grid-side waveforms, which show that the grid voltage stays sinusoidal with a peak magnitude of about 230 V to 250 V throughout the experiment. Electric vehicle (EV) battery charging and discharge circumstances cause a dynamic fluctuation in grid current. Power is actively transferred from the grid to the dc-link and battery during the first period from 0 to 0.2 s, when the grid current oscillates rather large, reaching roughly 60 A to 70 A. The current magnitude decreases from approximately 20 A to ±30 A between 0.2 s and 0.4 s, indicating a decrease in power demand. A light-load or transition area is indicated by the current becoming very tiny, near to 0 A, between 0.4 and 0.6 s. Confirming a resumption of power exchange with the battery, the current increases after 0.6 s and fluctuates between around 20 A and ±40 A. The front-end converter keeps the power quality and current shape excellent, as seen by the near-sinusoidal current profile. The solar source's contribution to the dc-link may be seen in the PV voltage and PV current charts. The photovoltaic voltage stays about 245-250 V from 0 to 0.4 s, the current drops to around 10 A from 0.2 s to 0.4 s, and the current drops to about 20 A from 0 to 0.2 s. By the time the simulation is over, the PV voltage has decreased from around 250 V to 130 V, and the PV current has dropped to almost 0 A at t = 0.4 s. It then gradually settles at 110-120 V. After 0.4 seconds, the PV source begins to supply less power, which suggests that the solar operating conditions or irradiance level have changed. Consequently, the grid and the EV battery, in their respective modes of operation, primarily support the dc-link. No matter what happens with the source or the load, the dc-link voltage Vdc stays regulated around its reference, proving that the control approach is working. The dc-link voltage quickly increases during startup, temporarily peaks at 470–480 V, and then settles at between 390 and 410 V. The dc-link voltage stays at 400 V with little ripple between 0.1 s and 0.8 s. At about 0.8 s, there is a little disruption, and the dc-link voltage spikes back up to around 440–450 V. It then drops back down to about 400–410 V. That the suggested control keeps the dc-bus well-regulated even when the power goes off is shown here. The waveforms on the EV side demonstrate the charging and discharging action in both directions.

Throughout the majority of the simulation, the voltage at the battery terminals of the electric vehicle (Vev) stays relatively consistent at roughly 104 V. As the time elapses from 0.6 s to 0.8 s, the voltage of the battery climbs to about 104.6-104.8 V, then drops somewhat after 0.8 s, and finally settles around 103.8-104 V. The EV current Iev provides a clearer confirmation of the operational modes. The EV current stays at 0 A from 0 to 0.6 s, suggesting either standby or very low charging current. In the grid-to-vehicle charging mode, energy is transferred into the EV battery when the current goes negative at about 0.6 s and lowers to almost -25 A. It subsequently drops even further to around -35 A at approximately 0.7 s. When the current changes to positive at about 0.8 s and reaches approximately 20 A, it reverses direction and climbs to around 35 A at 0.9 s, indicating that the car is transitioning to grid operation and the battery is recharging the system. This current reversal proves without a doubt that the suggested onboard charger can work in both directions. This pattern of activity is further corroborated by the EV SOC plot. Between 0 and 0.6 s, the SOC stays relatively steady at about 84.490%; at 0.8 s, when the charging period begins, it rises slightly at around 84.4915%. Consistent with the discharging or V2G interval, the SOC starts to slowly decline after 0.8 s and recovers to 84.490% by 1 s. Due to the limited duration of the simulation, the SOC fluctuation is tiny; nonetheless, the trend indicates that the two-way flow of battery energy is accurate. All things considered, the simulation results show that the suggested onboard charger works well and consistently even when things are changing. Controlled charging and discharging of the electric vehicle battery is made possible by the bidirectional push-pull stage, while the totem-pole front-end ensures a nearly sinusoidal input current and excellent dc-link voltage regulation. While the system is stable throughout mode changes, the PV source supports the dc-link in the first interval. Consequently, for cutting-edge G2V and V2G applications, the suggested architecture provides better power quality, dependable bidirectional energy transmission, and efficient integration of grid, PV, and EV battery systems.

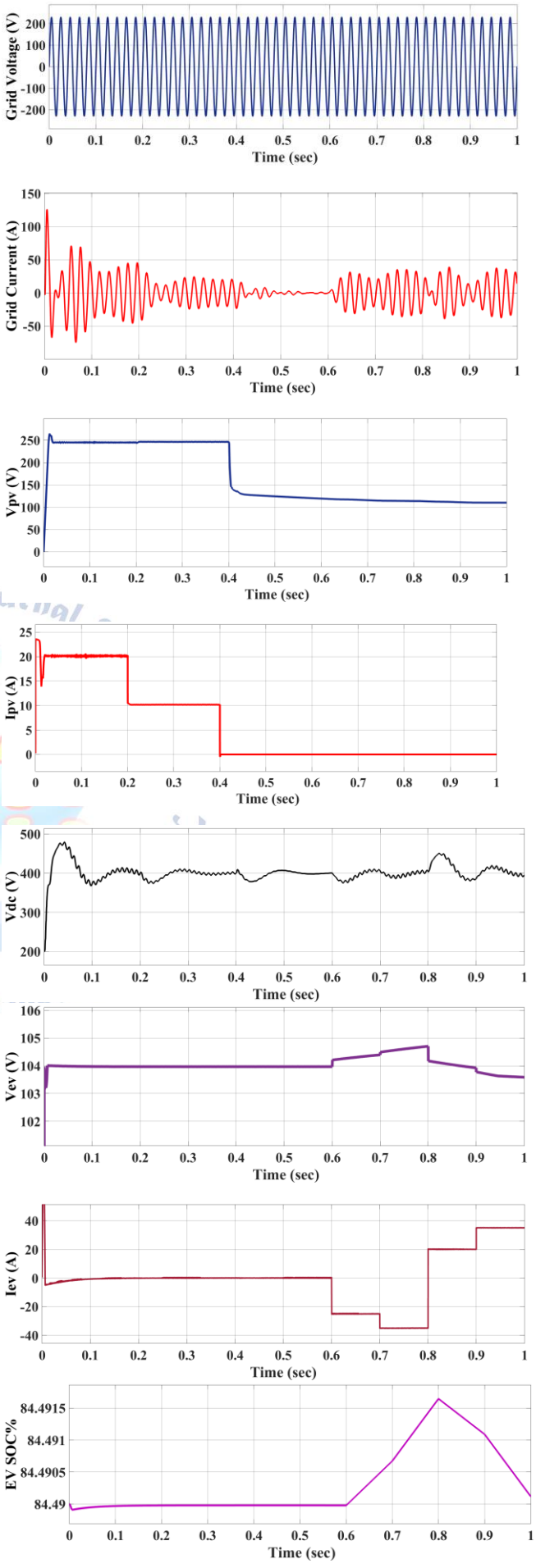

Fig.9 Simulation Results and Performance Analysis of the Proposed Bidirectional EV Onboard Charger

B. Power Factor Correction Performance of Totem-Pole Converter

By analyzing the power factor, we can confirm that the totem-pole converter is performing as expected in terms of power quality. Proper synchronization and good current shaping are shown by the waveform, which shows that the input current closely tracks the grid voltage. We keep the computed power factor at 0.985, which is close to one. As a result, reactive power consumption is reduced and overall system efficiency is improved, indicating that the proposed totem-pole converter accomplishes near-unity power factor correction.

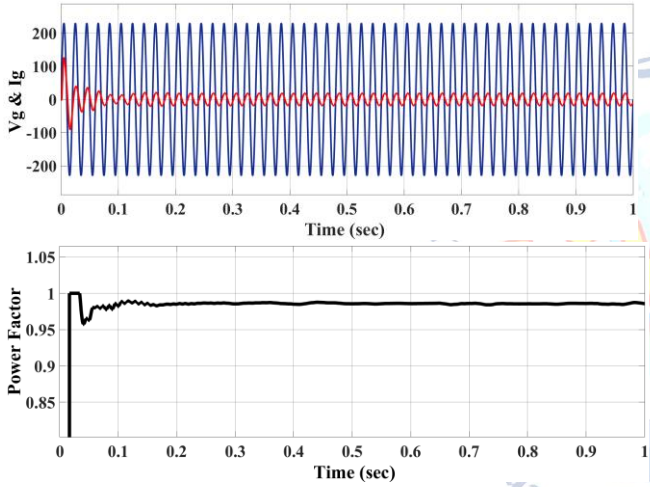

Fig.10 Simulation results of Power Factor Correction Performance of Totem-Pole Converter

C. Dynamic Power Variation and Energy Management under PV and EV Operating Conditions

The proposed grid-PV-EV system's dynamic power fluctuation is shown in kW for various solar and EV load circumstances. The data demonstrate that from 0 to 1 s, the grid, PV system, and EV battery all worked together to share electricity. In the first second, there is a transient where the grid power spikes to about 10 kW for a second before leveling down. During the starting time, the PV power settles around 4.5 kW to 5 kW, while the EV power stays near to 0 kW, meaning that the EV isn't actively exchanging power. The PV system provides about 5 kW and is the main source from 0 to 0.2 s. The grid power becomes negative at this time, fluctuating between -8 kW and -3 kW, which means that electricity is flowing back into the grid or being used less by the grid, depending on the convention for the signs. With electricity close to zero kilowatts, the EV stays idle. The decrease in solar output is shown by the PV power dropping to around 2.5 kW between 0.2 s and 0.4 s. The grid adjusts its power output to match this decrease, which ranges from around -5 kW to -2 kW. During this time, the EV will not move from its idle state. The PV output drops even lower to approximately 0 kW between 0.4 s and 0.6 s, suggesting that the solar contribution is minor at best. At this time, the electric vehicle power is almost nonexistent, and the grid power is close to zero kilowatts, indicating a balanced or low demand state. The EV begins to be involved in the system at around 0.6 seconds. Charging mode (grid-to-vehicle) is indicated when the EV power becomes negative, reaching around −2.5 kW to −3.5 kW. The necessary energy for charging the batteries is supplied when the grid power becomes marginally positive, ranging from zero to one kilowatt-hour. In the time between 0.6 s and 0.8 s, the electric vehicle (EV) keeps charging, and its power fluctuates between -3 kW and -4 kW, all the while the grid provides the required electricity to keep the system balanced. The PV contribution is rather low within this time frame. During vehicle-to-grid (V2G) operation, the electric vehicle's power changes from negative to positive at about 0.8 s, increasing from around 2 kW to 3.5 kW. This occurs when the electric vehicle's battery sends power back to the system. Similarly, there is a decrease in reliance on the grid when the grid power becomes negative once again, fluctuating about between -3 kW and -5 kW. The EV keeps discharging between 0.8 and 1 s, and the system keeps the power flow balanced among the sources. The grid makes real-time adjustments to keep everything in balance, and the PV power stays almost at zero. The findings show that the proposed system takes kW dynamic power sharing into account well, allowing for seamless changes between PV production, grid support, and EV charging/discharging modes. This technology has shown itself suitable for bidirectional V2G applications with effective power management by achieving coordinated operation under variable solar and EV load circumstances.

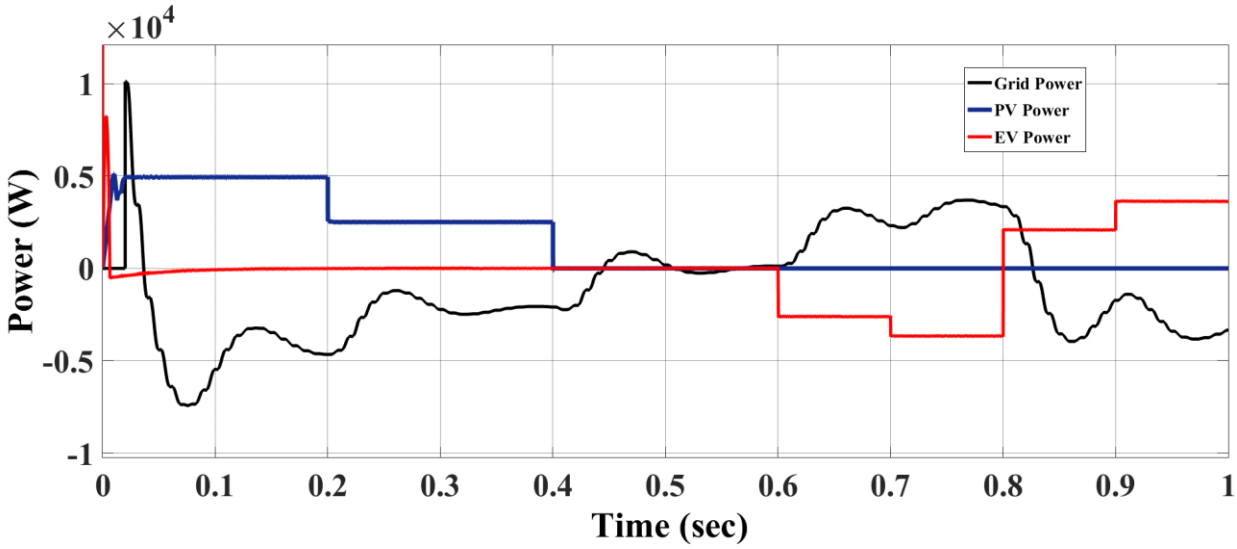

Fig.11 Simulation results of Dynamic Power Variation and Energy Management under PV and EV Operating Conditions

9. Conclusion

Using an interleaved totem-pole AC-DC converter and a bidirectional push-pull DC-DC stage, this research demonstrated a bidirectional EV onboard charger that maximizes power quality for vehicle-to-grid (V2G) applications. By cutting out the traditional diode bridge rectifier and streamlining the power conversion process, the suggested architecture improves efficiency, power density, and overall performance while reducing conduction losses. High power quality at the grid interface is guaranteed by the totem-pole front-end converter, which delivers a power factor close to unity (around 0.985) with minimal input current distortion, according to the simulation findings. For more dependable and economical operation, the interleaved structure enhances thermal performance and decreases current ripple. The DC-link voltage is consistently controlled throughout different operating situations, which proves that the control technique is working as intended. Effortless switching between grid-to-vehicle (G2V) and vehicle-to-grid (V2G) modes proves the suggested system can work in both directions. With consistent voltage and current profiles, the electric vehicle battery is charged and discharged in a regulated way under circumstances of constant current and voltage. Further evidence of effective grid, PV (if integrated), and EV coordination is provided by the dynamic power variation findings, which guarantee a balanced flow of power under varying demand and generation conditions. All things considered, the onboard charger that has been suggested provides a future-proof, effective, and adaptable option for electric vehicle charging infrastructure. It is ideal for smart grid and grid-interactive electric vehicle applications because it greatly improves power quality, decreases losses, and allows efficient bidirectional energy transmission. To further enhance system speed and scalability, future work may concentrate on optimizing sophisticated controls and implementing hardware.

Conflict of interest statement

Authors declare that they do not have any conflict of interest.

REFERENCES

[1] S. S. G. Acharige, Md. E. Haque, M. T. Arif, N. Hosseinzadeh, K. N. Hasan, and A. M. T. Oo, ''Reviewof electric vehicle charging technologies, standards, architectures, and converter configurations,'' IEEE Access, vol. 11, pp. 41218–41255, 2023, doi: 10.1109/ACCESS.2023.3267164.

[2] A. Khaligh and M. D'Antonio, ''Global trends in high-power on-board chargers for electric vehicles,'' IEEE Trans. Veh. Technol., vol. 68, no. 4, pp. 3306–3324, Apr. 2019, doi: 10.1109/TVT.2019.2897050.

[3] R. Pradhan, N. Keshmiri, and A. Emadi, ''On-board chargers for highvoltage electric vehicle powertrains: Future trends and challenges,'' IEEE Open J. Power Electron., vol. 4, pp. 189–207, 2023, doi: 10.1109/OJPEL.2023.3251992.

[4] H. Nazi, E. Babaei, S. Tohidi, and M. Liserre, ''An isolated SRC-based single phase single stage battery charger for electric vehicles,'' IEEE Trans. Transport. Electrific., vol. 9, no. 1, pp. 1252–1262, Mar. 2023, doi: 10.1109/TTE.2022.3185018.

[5] D. Zinchenko, A. Blinov, A. Chub, D. Vinnikov, I. Verbytskyi, and S. Bayhan, ''High-efficiency single-stage on-board charger for

electrical vehicles,'' IEEE Trans. Veh. Technol., vol. 70, no. 12, pp. 12581–12592, Dec. 2021, doi: 10.1109/TVT.2021.3118392.

[6] S.-G. Jeong, Y.-S. Jeong, J.-M. Kwon, and B.-H. Kwon, ''A soft-switching single-stage converter with high efficiency for a 3.3-kW on-board charger,'' IEEE Trans. Ind. Electron., vol. 66, no. 9, pp. 6959–6967, Sep. 2019, doi: 10.1109/TIE.2018.2877093.

[7] S. S. Sayed and A. M. Massoud, ''Review on state-of-the-art unidirectional non-isolated power factor correction converters for short-/long-distance electric vehicles,'' IEEE Access, vol. 10, pp. 11308–11340, 2022, doi: 10.1109/ACCESS.2022.3146410.

[8] R. Pandey and B. Singh, ''Canonical switching cell (CSC) converterbased power factor-corrected battery charger for e-rickshaw,'' IEEE Trans. Ind. Appl., vol. 56, no. 5, pp. 5046–5055, Sep. 2020, doi: 10.1109/TIA.2020.2996539.

[9] R. Kushwaha, V. Khadkikar, and A. Edpuganti, ''Electric vehicle onboard fast charging through converter maximum switch utilization,'' IEEE Trans. Power Electron., vol. 39, no. 1, pp. 998–1014, Jan. 2024, doi: 10.1109/TPEL.2023.3321760. 121566

[10] G. K. Naveen Kumar, A. K. Verma, and N. Sandeep, ''Improved gain single-phase buck-boost PFC with wide output voltage range for universal input EV applications,'' IEEE Trans. Ind. Electron., vol. 72, no. 1, pp. 299–307, Jan. 2025.

[11] R. Patil and S. P. Prakash, ''Performance enhancement of switchedcapacitor- based bridgeless buck PFC rectifier,'' IEEE Trans. Power Electron., vol. 39, no. 3, pp. 2938–2942, Mar. 2024, doi: 10.1109/TPEL.2023.3340701.

[12] G. Li, D. Yang, B. Zhou, Y.-F. Liu, and H. Zhang, ''A topology reconfigurable fault-tolerant two-and-single stage AC–DC converter for high reliability applications,'' IEEE Trans. Ind. Electron., vol. 70, no. 4, pp. 3708–3716, Apr. 2023, doi: 10.1109/TIE.2022.3174236.

[13] S. R. Meher and R. K. Singh, ''A standard two stage on-board charger with single controlled PWM and minimum switch count,'' IEEE Trans. Ind. Appl., vol. 59, no. 4, pp. 4628–4639, Jul. 2023, doi: 10.1109/TIA.2023.3267334.

[14] J. Lu, A. Mallik, S. Zou, and A. Khaligh, ''Variable DC-link control loop design for an integrated two-stage AC/DC converter,'' IEEE Trans. Transport. Electrific., vol. 4, no. 1, pp. 99–107, Mar. 2018, doi: 10.1109/TTE.2017.2755772.

[15] P. Dadhaniya, M. Maurya, and G. M. Vishwanath, ''A bridgeless modified boost converter to improve power factor in EV battery charging applications,'' IEEE J. Emerg. Sel. Topics Ind. Electron., vol. 5, no. 2, pp. 553–564, Apr. 2024, doi: 10.1109/JESTIE.2024.3355887.

[16] L. Xue, Z. Shen, D. Boroyevich, P. Mattavelli, and D. Diaz, ''Dual active bridge-based battery charger for plug-in hybrid electric vehicle with charging current containing low frequency ripple,'' IEEE Trans. Power Electron., vol. 30, no. 12, pp. 7299–7307, Dec. 2015, doi: 10.1109/TPEL.2015.2413815.

[17] S. A. Assadi, H. Matsumoto, M. Moshirvaziri, M. Nasr, M. S. Zaman, and O. Trescases, ''Active saturation mitigation in high-density dual-activebridge DC–DC converter for on-board EV charger applications,'' IEEE Trans. Power Electron., vol. 35, no. 4, pp. 4376–4387, Apr. 2020, doi: 10.1109/TPEL.2019.2939301.

[18] V. R. K. Kanamarlapudi, B.Wang, N. K. Kandasamy, and P. L. So, ''A new ZVS full-bridge DC–DC converter for battery charging with reduced losses over full-load range,'' IEEE Trans. Ind. Appl., vol. 54, no. 1, pp. 571–579, Jan. 2018, doi: 10.1109/TIA.2017.2756031.

[19] N. Hou, Y. Zhang, and Y. W. Li, ''A natural transient-behavior-based control theory for DAB-based two-stage DC–DC converter,'' IEEE Trans. Power Electron., vol. 38, no. 12, pp. 15137–15141, Dec. 2023, doi: 10.1109/TPEL.2023.3316642.

[20] S. Harinaik, S. Sathyan, and N. J. M. Mary, ''Design and analysis of modified series–parallel quasiresonant half-bridge DC/DC converter for renewable energy applications,'' IEEE J. Emerg. Sel. Topics Ind. Electron., vol. 5, no. 3, pp. 1089–1099, Jul. 2024.